

The Effect of Carbon Nanotube Hydrophobicity on the Mechanical Properties of Carbon Nanotube-Reinforced Thermoplastic Polyurethane Nanocomposites

Simon Smart,^{1,3} David Fania,² Adriyan Milev,² G. S. Kamali Kannangara,² Max Lu,³ Darren Martin³

¹School of Chemical Engineering, The University of Queensland, Brisbane, QLD 4072, Australia

²School of Natural Sciences, University of Western Sydney, Locked Bag 1797, Penrith South DC 1797, Australia

³ARC Centre for Functional Nanomaterials, Australian Institute for Bioengineering and Nanotechnology, The University of Queensland, Brisbane, QLD 4072, Australia

Received 14 April 2009; accepted 13 July 2009

DOI 10.1002/app.31115

Published online 2 March 2010 in Wiley InterScience (www.interscience.wiley.com).

ABSTRACT: Double walled carbon nanotubes (DWNT) were functionalized by reacting methanol, dodecylamine, or octadecylamine with a toluene 2,4-diisocyanate linker through a two-stage reaction procedure. TGA coupled with FTIR analysis of both the decomposition products and the DWNT samples demonstrated that the functionalization procedure was successful and proceeded as expected for all samples. A preliminary investigation of the reinforcing

capabilities of the functionalized DWNT in a thermoplastic polyurethane host polymer was then conducted. Tensile testing of the resultant nanocomposites demonstrated that the octadecylamine functionality provided the greatest enhancement in tensile strength and toughness. © 2010 Wiley Periodicals, Inc. *J Appl Polym Sci* 117: 24–32, 2010

Key words: nanocomposites; polyurethanes

INTRODUCTION

The polymer industry is continually investigating new materials that offer increased performance at lower costs, often necessitating the introduction of fillers. Nanoparticles offer significant advantages over macro- or microsized fillers, including a greater surface area to mass ratio, low percolation threshold (both electrical and rheological) and often very high aspect ratios, and as such there has been significant research and investment into the production of polymeric nanocomposites. One of the most commonly investigated nanofillers, carbon nanotubes (CNT), are unique, one-dimensional macromolecules, possessing high tensile strengths, low density and excellent thermal and chemical stability.^{1,2}

Current research has shown that, despite the much publicized potential of CNT, nanocomposites made from pristine CNT have failed to yield the expected property enhancements. The most commonly cited reasons include poor dispersion of

individual CNT and poor interfacial interactions between the CNT and the host polymer.³ Computational^{4,5} and experimental^{6–9} studies have indicated that covalent attachment of functional groups to CNT sidewalls can have a profound effect on polymer to CNT interfacial load transfer⁴ and overall bulk reinforcement.^{6–9} Both short⁷ and long chain^{8,9} functional groups have shown successful reinforcement of polymer matrices, suggesting that both hydrogen bonding and polymer entanglement may aid load transfer between host polymer and CNT. Functionalization of CNT sidewalls has also been demonstrated to improve dispersion in common polymer solvents.^{10,11} CNT surface modifiers are typically either short hydrophilic groups capable of significant hydrogen bonding with the host polymer⁷ or long chain hydrophobic groups designed to break apart CNT aggregates and increase dispersion.⁶ The ideal surface modifications would balance the entropic effects needed for breakdown of CNT aggregates and increased dispersion against the enthalpic effects needed for enhanced interactions at the polymer/CNT interface. This balanced approach should be particularly effective for thermoplastic polyurethane- (TPU) based nanocomposites given their distinct phase-separated morphology, where hydrophilic hard segments and hydrophobic soft segments provide readymade sequences to interact with. This approach is currently unexplored in the TPU/CNT nanocomposite literature.

Correspondence to: D. Martin (darren.martin@uq.edu.au).

Contract grant sponsors: ARC Centre for Functional Nanomaterials and the Department of Chemical Engineering Super Scholarship, The functionalization and TGA/FTIR work was completed at University of Western Sydney, Australia.

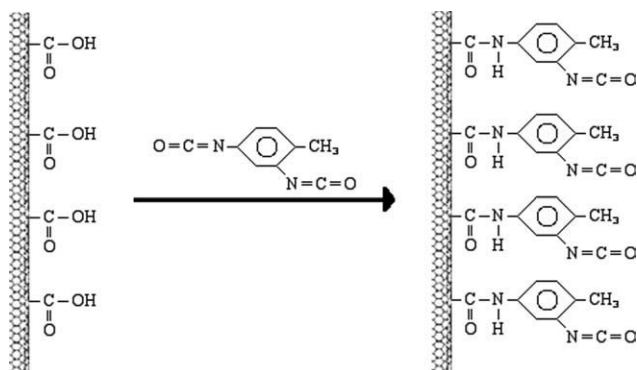


Figure 1 Reaction scheme for attachment of isocyanate functionality (Modified from Ref. 11).

Zhao et al.¹¹ reported the functionalization of MWNT with isocyanate groups through the reaction scheme shown in Figure 1. The method proved successful at increasing dispersion of MWNT in anhydrous toluene,¹¹ although there have been no published studies into the effect of the functionalization on polymeric nanocomposites. Applied to TPUs, the free isocyanate groups should provide an enthalpic driving force, by drawing in hard segments, to increase interfacial interaction. However, there is no driving force for increased CNT dispersion, in fact, isocyanate groups are highly reactive and, in the presence of $-\text{OH}$ functional groups will form covalent bonds between individual CNT, ultimately increasing aggregation.

To increase dispersion, it was decided to covalently attach long chain alkyl amines or alcohols to the free isocyanate group in a second reaction (as shown in Fig. 2). The urea or urethane linkages formed should still attract and interact with the hydrophilic hard segments of the TPU, whereas the steric hindrance of the alkyl tails should aid in dispersion of individual CNT throughout the host polymer matrix.

There have been no published studies into the effects of CNT alkyl functional group length or conformation. Thus, to determine the effect of alkyl chain length and subsequently decide on the optimal CNT surface functionality, a series of trials were performed using methanol, dodecylamine, and octadecylamine as the second stage reactant. The proposed reaction schemes are shown in Figure 2.

It was hypothesized that the covalent functionalization of the CNT surface with functional groups that contained both a hydrophobic and hydrophilic component would improve the tensile properties of resultant TPU-based nanocomposites. Further to this, it was hypothesized that functional groups with longer hydrophobic alkyl tails would enhance the tensile properties of resultant TPU-based nanocomposites more than functionalized groups with shorter alkyl tails.

EXPERIMENTAL

Functionalization

DWNT were synthesized through a semicontinuous arc-discharge technique described previously.^{12,13} They were purified through an acid wash process, which introduced carboxylic acid groups along the DWNT sidewalls.¹⁴ A full characterization of the DWNT starting material (i.e., before functionalization with TDI but after acid purification) has already been performed.¹⁵ The functionalization of the DWNT sample was performed in a two-stage reaction process. The first stage consisted of reacting toluene 2,4-diisocyanate (TDI) with DWNT for 2 h in a CEM Discover LabMate microwave reactor fitted with internal temperature and pressure controls and a power control up to 300 W. The 100 mL reaction chamber was lined with Teflon PFA[®] with an operating range of 0–200°C and 0–200 psi. Typically, 50 mg of CNT sample (dried overnight at 100°C under vacuum) was added to 5 mL of acetone (CHROMASOLV \geq 99.9%, Aldrich) in the reaction vessel. The sealed reaction vessel was then evacuated of air, and dry N₂ gas was added. Diluted toluene 2,4-diisocyanate (TDI) (purum grade \geq 98.0%, Fluka) in acetone was then transferred into the tube to give a 20% stoichiometric excess of TDI. The reaction vessel was then placed into the microwave reactor for 2 h at a power of 100 W under constant stirring (temperature stabilized at \sim 85°C, whereas pressure stabilized at \sim 180 kPa).

The second stage of functionalization involved the covalent attachment of methanol, dodecylamine, or octadecylamine to the TDI-modified CNT samples. Typically 20–50% stoichiometric excess of reactant [methanol (anhydrous \geq 99.8%, Aldrich), dodecylamine (purum grade \geq 98%, Fluka; 8 g dissolved in 100 mL of acetone (CHROMASOLV \geq 99.9%, Aldrich)] or octadecylamine (technical grade \geq 90%, Fluka; 8 g dissolved in 100 mL of acetone (CHROMASOLV \geq 99.9%, Aldrich))) was added to the reaction vessel. The reaction vessel was then placed in an ultrasonic bath (Bronson 1210) at 60°C for 90 min. The reaction mixture was then transferred to Eppendorf microfuge tubes, which were then centrifuged (Eppendorf Centrifuge 5417C) at 10,000 rpm for 5 min. The supernatant was then removed, and the CNT were washed with 0.5 mL of acetone (per tube) and sonicated for 2 min at 60°C. This washing process was then repeated using toluene (ACS reagent \geq 99.5%, Sigma-Aldrich). Samples were then dried in an oven at 110°C. The resultant samples were labeled DWNT-TDI-CH₃, DWNT-TDI-C₁₂, and DWNT-TDI-C₁₈, respectively.

Fourier-transform infra-red spectroscopy

FTIR spectroscopy of samples was performed on a Bruker Vertex 70 FTIR spectrometer. Samples were

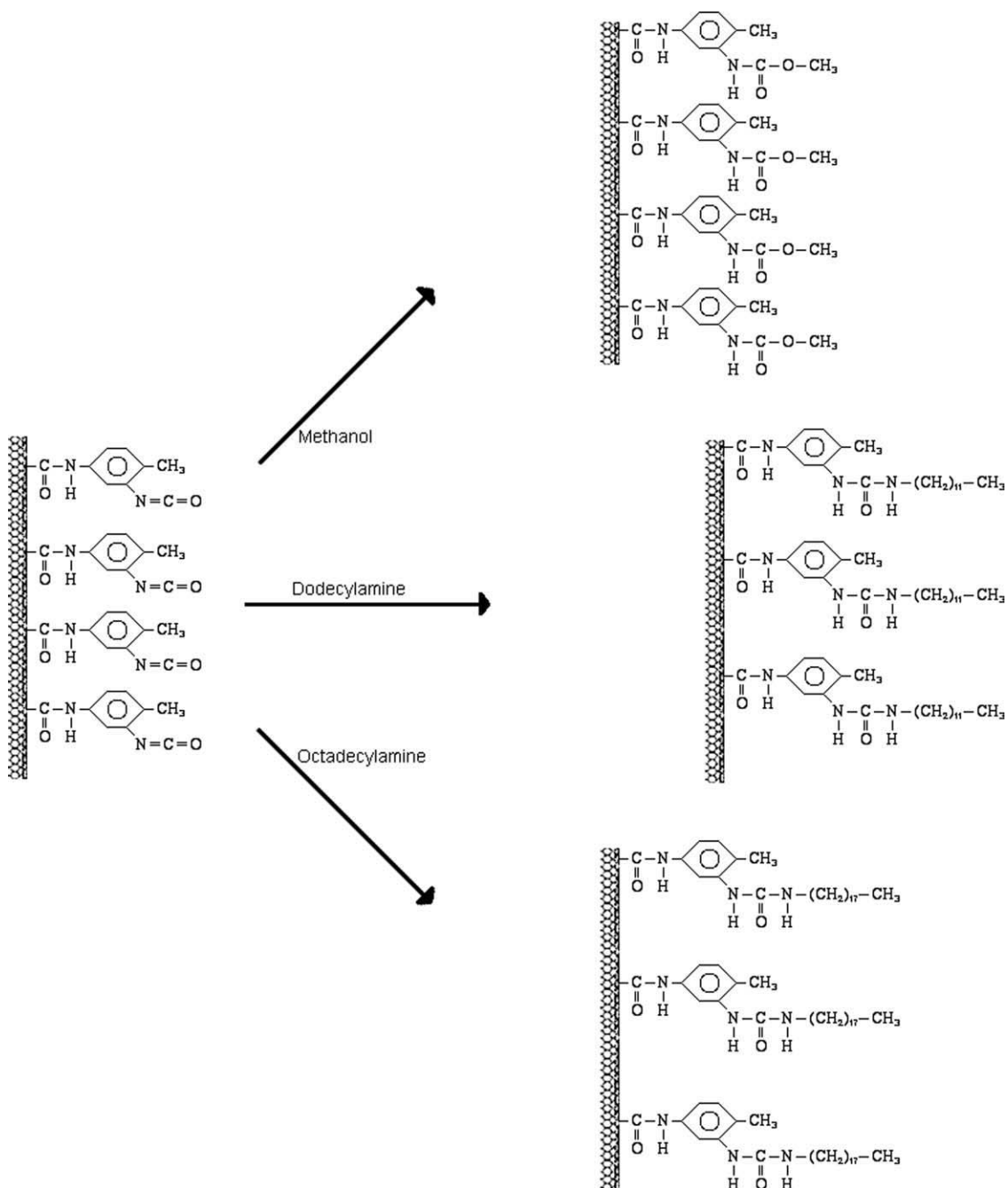


Figure 2 Reaction scheme(s) for attachment of alkyl chain functionalities.

prepared by grinding 0.5 mg of sample with ~200 mg of KBr before being converted into disk form under high pressure. Samples were scanned 16 times at a resolution of 1 cm^{-1} .

Thermogravimetric analysis

DSC-TGA/FTIR experiments were performed on a NETZSCH STA 449C coupled to a Bruker Vertex 70 FTIR spectrometer. Each sample was heated from 20 to 750°C at a rate of $10^\circ\text{C}/\text{min}$ in argon with a flowrate of 25 mL/min. Mass loss, differential scan-

ning calorimetric data, and gas-phase infrared spectra were recorded.

Nanocomposite preparation

Each functionalized sample (10 mg) was sonicated in 2 mL of *N,N*-dimethylformamide (DMF) (anhydrous 99.8%, Aldrich) for 5 min in an ultrasonic bath. This solution was then mixed with 20 mL of TPU (dissolved at 5 wt % in tetrahydrafuran (THF) (anhydrous 99.8%, Aldrich) and sonicated for a further 5 min. The mixture was then transferred to 80 mm

glass Petri dishes and left to evaporate in a desiccator for 72 h, before being annealed at 70°C in a vacuum for 12 h.

Mechanical testing

Tensile tests were performed on an Instron model 4505 universal testing machine at 25°C. Dumbbells were punched from an ASTM D-638-M-3 die, and five replicates of each sample were used. Young's modulus was calculated from the slope of the tensile curve at 0–10% strain.

RESULTS AND DISCUSSION

Thermogravimetric analysis of carbon nanotubes in an inert atmosphere is commonly used to investigate the composition and thermal stability of surfactant coated or covalently functionalized CNT. It was used in this study, in conjunction with gas-phase FTIR, to provide a detailed evaluation of the functionalization procedure.

Figure 3 demonstrates that the functionalized CNT samples underwent two distinct mass losses between 200 and 550°C. The temperature associated with the onset of the first mass loss varied between 170 and 200°C, whereas the onset temperature for the second mass loss varied between 340 and 435°C depending on the sample. As each functionalized sample displayed distinctly different onset temperatures for each mass loss, the respective TGA derivative (dTGA) curves were deconvoluted into their constituent peaks (summarized in Table I) and analyzed in conjunction with the time resolved gas-phase FTIR data to better understand the decomposition process.

The DWNT-TDI-CH₃ sample showed three constituent dTGA peaks, which, when analyzed in conjunction with the time resolved gas-phase FTIR spectrum (Fig. 4), indicated that various hydrocarbons

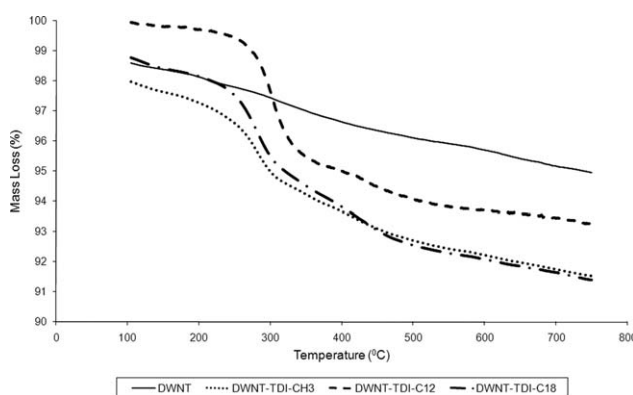


Figure 3 Representative TGA curves for DWNT samples with various surface functionalities (inert atmosphere).

TABLE I
Summary of dTGA Data

Sample name	dTGA Peak 1 (°C)	dTGA Peak 2 (°C)	dTGA Peak 3 (°C)
pDWNT-TDI-CH ₃	210	290	460
pDWNT-TDI-C ₁₂	315	420	
pDWNT-TDI-C ₁₈	355	450	

and CO₂ were the main decomposition products of the sample.

The initial dTGA peaks at ~ 210 and 290°C correspond to the initial C–H stretching peak in Figure 5(a) and the major peak in the CO₂ evolution profile in Figure 5(b), respectively. These results suggest this initial mass loss is associated with the loss of hydrocarbon material; however, the low temperature at which these species evolved implied that this initial mass loss was most likely associated with desorption and partial decomposition of the CH₃–TDI–CH₃ by product. The final dTGA peak at ~ 460°C corresponds to the major peak in the CH₂ evolution profile, indicating this mass loss was primarily associated with the decoupling and decomposition of the TDI–CH₃ functionality.

The DWNT-TDI-C₁₂ sample showed two constituent dTGA peaks at 315 and 420°C and a complex decomposition profile (Fig. 6) with hydrocarbons [both aliphatic in Fig. 7(a) and aromatic in Fig. 7(b)] and CO₂ identified by FTIR as the major species. However, unlike the DWNT-TDI-CH₃ sample, these evolution profiles do not correlate well with the major mass loss peaks in the dTGA profile. The evolution profiles appear to lag significantly behind the

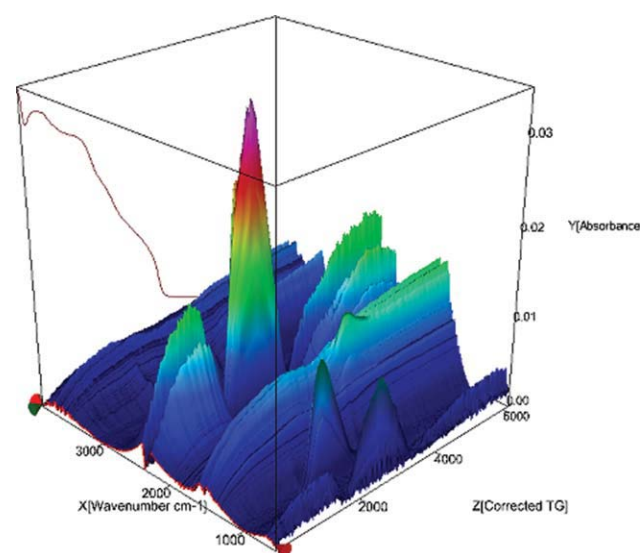


Figure 4 Time resolved TGA/FTIR spectrum for the DWNT-TDI-CH₃ sample. [Color figure can be viewed in the online issue, which is available at www.interscience.wiley.com.]

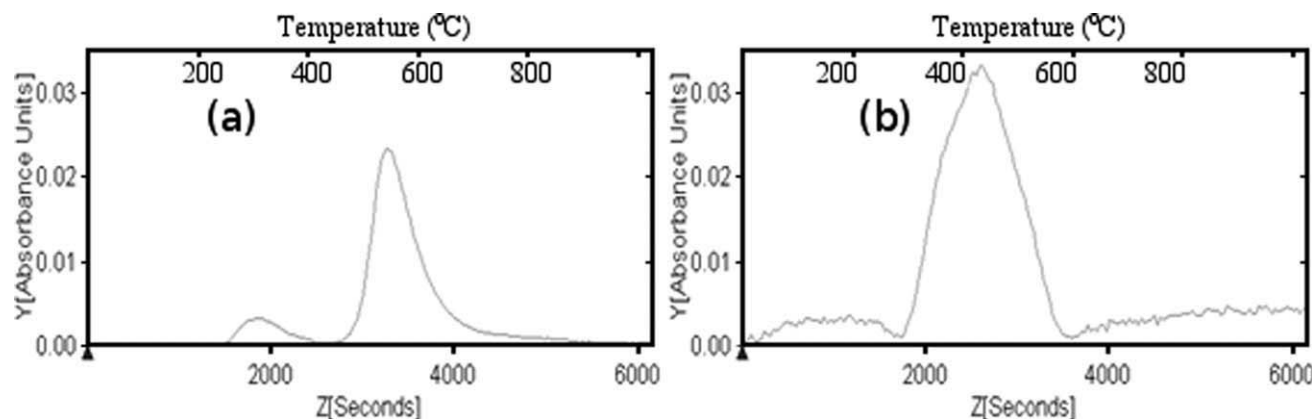


Figure 5 Evolution profile for CH_2 (a) and CO_2 (b) species in the DWNT-TDI- CH_3 sample.

major mass losses, peaking at $\sim 520^\circ\text{C}$ and 600°C for the aliphatic and aromatic hydrocarbon species, respectively.

It was hypothesized that the most probable cause was condensation of the high molecular weight decomposition products (aliphatic hydrocarbons associated with the C_{12} tail) before they could reach the FTIR detector. The FTIR detector is not located within the furnace of the TGA, instead the decomposition products are carried to the detector through a heated, sealed tube by an argon purge. The temperature of the tube is held constant at 200°C , regardless of the furnace temperature. Hence, it is possible that high molecular weight compounds leave the TGA furnace as a gas but condense inside the tube, before reaching the FTIR detector.

It is postulated that the decomposition of the TDI- C_{12} functionalities occurred predominantly through a two-stage process. The first stage involved the cleavage of the aliphatic tail at or above the urea linkage and most likely resulted in the release of C_{12} or smaller aliphatic hydrocarbons. It is further postulated that the high molecular weight of these hydrocarbons caused the majority to condense inside the tube connecting the furnace and FTIR detector. Hence, at the actual mass loss temperature, only a small fraction of these decomposition products would have passed through the detector. However, as the temperature of the furnace and, as a result, the purge gas increased, it is suggested that an increasing number of hydrocarbon molecules made it to the detector before condensing. It is also suggested that on condensation, some of these larger aliphatic hydrocarbons may have fallen (under the influence of gravity) back into the TGA furnace to undergo further decomposition into smaller hydrocarbon fragments which would then easily pass through to the detector. Both these explanations result in the shifting of the aliphatic hydrocarbon peak [Fig. 7(a)] higher than the original mass loss temperature. The second stage involved the cleavage

of the remaining aromatic portion at the C–N bond in the amide linkage. As with the aliphatic hydrocarbons, the high molecular weight of these aromatic compounds was the most likely cause for the upshift in peak evolution temperature. Figure 6 demonstrates the presence of CO at $\sim 750^\circ\text{C}$, which provides further evidence for cleavage at the C–N bond. This proposed mechanism is consistent with the two-stage weight loss seen in Figure 3 and is further corroborated by the Gram-Schmidt analysis, which provides the integral of the FTIR spectrum per time point. As seen with the aliphatic and aromatic hydrocarbon peaks, the Gram-Schmidt curve (not shown) is shifted upward of the major mass loss temperatures. This result implied that either the decomposition products are not detectable through FTIR (which given the possible species present is exceedingly remote) or have been delayed in reaching the FTIR detector.

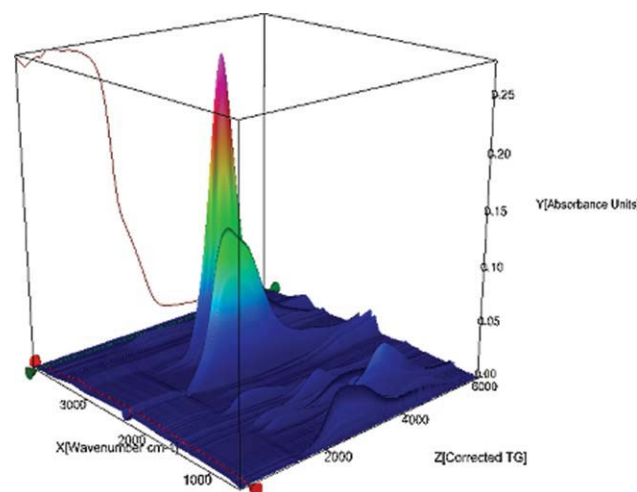


Figure 6 Time resolved TGA/FTIR spectrum for the DWNT-TDI- C_{12} sample. [Color figure can be viewed in the online issue, which is available at www.interscience.wiley.com.]

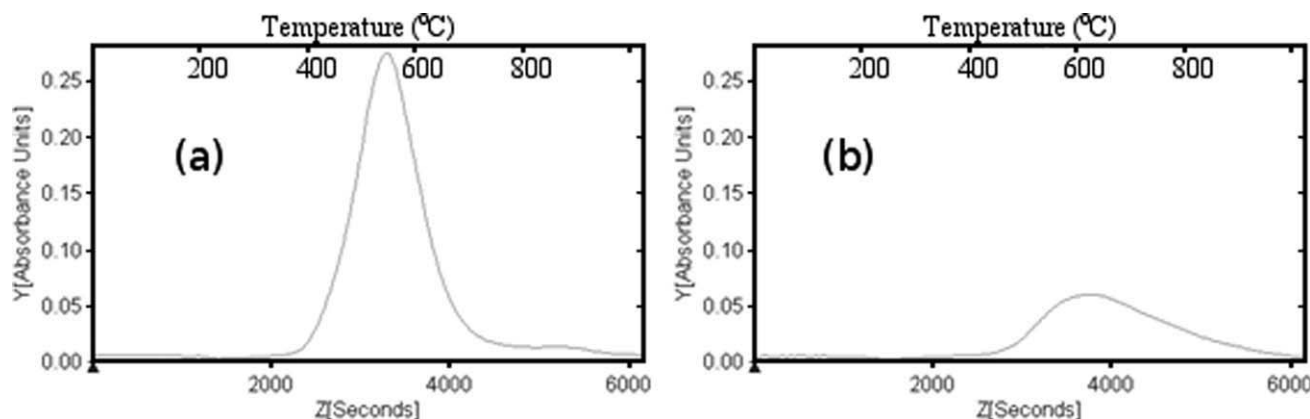


Figure 7 Evolution profile for aliphatic (a) and aromatic (b) hydrocarbon species in the DWNT-TDI-C₁₂ sample.

The DWNT-TDI-C₁₈ sample showed two constituent dTGA peaks at 355 and 450°C and a complex decomposition profile (Fig. 8) with aliphatic and aromatic hydrocarbons identified, along with CO₂, as the major species (Fig. 9).

As demonstrated in the DWNT-TDI-C₁₂ sample, the evolution profile and deconvoluted dTGA peaks did not display good correlation. Instead the major peak in the evolution profile of the aliphatic hydrocarbons (the major species present) was again shifted to a higher temperature (~600°C) than either of the major mass loss peaks. These results were consistent with the proposed decomposition mechanism for the DWNT-TDI-C₁₂ sample.

The time resolved TGA/FTIR spectra for all DWNT functionalized samples provide significant evidence that the functionalization procedure was successful and that it proceeded as predicted in Figures 1 and 2.

To determine the success of the functionalization procedure, the conversion of carboxylic acid groups to TDI-C_X functional groups was calculated as shown in eq. (1).

$$TC_{mass} = \frac{FC_A}{FC_T} \quad (1)$$

where TC_{mass} is the total conversion (on a mass basis) of carboxylic groups to the relevant end functionality, FC_A is the actual functional group content (wt %) as measured by TGA and FC_T is the theoretical functional group content (wt %), calculated by assuming 100% conversion of carboxylic acid groups to TDI (as shown in Fig. 1) followed by 100% conversion of free isocyanate groups to the relevant end functionality (as shown in Fig. 2). Although FC_A provides an initial measure of functional content, differences in the molecular weight of the TDI-C_X functional groups, make it an ineffective tool for comparison between samples. Thus, to allow direct comparison among the DWNT-TDI-CH₃, DWNT-

TDI-C₁₂ and DWNT-TDI-C₁₈ samples, the effective functionalization of the TDI-C_X functional group per mass of CNT was calculated as shown in eq. (2).

$$\text{Effective functionalization} = \frac{FC_A}{M_W(1 - FC_A - M_I)} \quad (2)$$

where, FC_A is the actual functional group content (wt %) as measured by TGA, M_I is the mass fraction of impurities as calculated by TGA in a previous study,¹⁵ and M_W is the molecular weight of the functional group. Analysis of the data (summarized in Table II) showed a minor trend whereby effective functionalization was decreased with increasing functional group size. There are many possible explanations for this observed trend including steric induced variations in reaction kinetics and/or poor availability of reactive sites for functionalization.

When considering the reaction sequence, the effects of steric hindrance of the reactant molecules

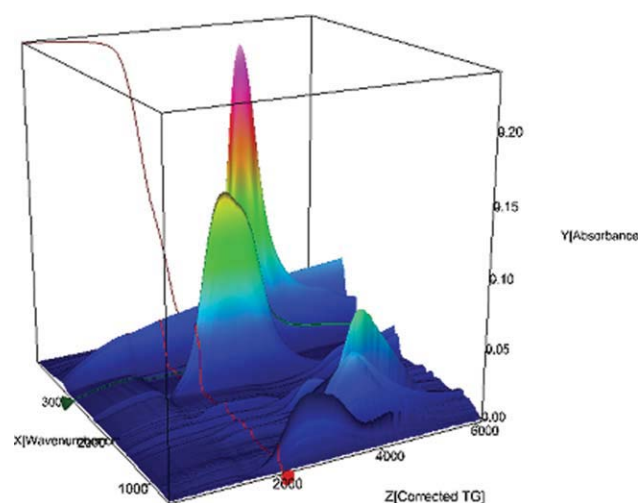


Figure 8 Time resolved TGA/FTIR spectrum for the DWNT-TDI-C₁₈ sample. [Color figure can be viewed in the online issue, which is available at www.interscience.wiley.com.]

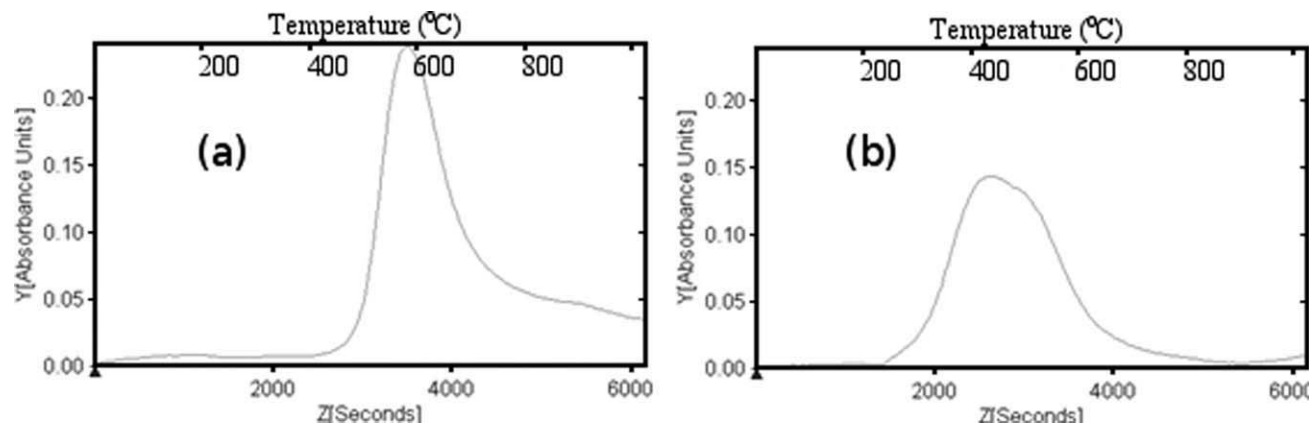


Figure 9 Evolution profile for CH_2 (a) and CO_2 (b) species in the DWNT-TDI- C_{18} sample.

are twofold. First, the bulkier reactants may have slowed the reaction kinetics resulting in a reduced conversion for the second stage of reaction. The reaction of isocyanates with amines is typically very rapid; however, it is possible that the reaction rate of the bulky dodecylamine and octadecylamine with the isocyanate functionalized DWNT was much slower than anticipated. As a result, the conversion for the second stage coupling may have been reduced in these samples when compared with the much smaller methanol (despite the comparatively slower reaction kinetics of isocyanates with alcohols). Second, it is postulated that some of the reactive defect sites along the DWNT sidewall may have been inaccessible to the larger reactant molecules due to the strong intertubular forces and high CNT bundling efficiency.¹⁶ That is, if the intertubular distance is smaller than the radius of gyration of TDI, methanol, dodecylamine, or octadecylamine, then it is feasible that some of the carboxylated reaction sites may actually have been inaccessible for further functionalization. As the radius of gyration increases with increasing tail length, the degree of coupling would be expected to decrease with increasing alkyl chain size, as was observed. However, the complexity of the various reaction sequences and the difficulty in discerning the location of the attached moieties made it impossible to establish the veracity of

these hypotheses. Indeed, the most likely explanation for the variation in effective functionalization rests with the well-publicized variations in CNT properties, in this case the $-\text{COOH}$ content, even amongst samples taken from the same batch.^{17,18}

FTIR was used in this study to confirm covalent bonding of the functional groups to the CNT surface as per the reaction scheme proposed in Figure 2. The unmodified DWNT spectrum [Fig. 10(a)] was used as a background. The peak at 1580 cm^{-1} was assigned to the $\text{C}=\text{C}$ stretching mode, inherent to the structure of all CNT.¹¹ The peak at 1717 cm^{-1} was assigned to the $\text{C}=\text{O}$ stretching mode of the carboxylic acid functional groups present on the CNT surface.^{11,19} The peaks at 2920 cm^{-1} and 2850 cm^{-1} were related to $\text{C}-\text{H}$ stretching of CH_2 groups found at nonoxidized defect sites in the CNT sidewalls.^{11,19} Peaks at $\sim 2360\text{ cm}^{-1}$ and 2340 cm^{-1} were assigned to CO_2 present in the FTIR chamber.¹⁹

The DWNT-TDI- CH_3 sample [Fig. 10(b)] showed a weak peak at 1617 cm^{-1} and a peak at 1540 cm^{-1} , which were assigned to the Amide I and II vibrations, respectively, in the secondary amide linkage^{19,20} formed when the TDI reacted with the carboxylic acid groups on the CNT surface as shown in Figure 1. The peak at 1696 cm^{-1} was assigned to the urethane linkage formed when the methanol reacted with free isocyanate groups as shown in Figure 2.

TABLE II
Summary of TGA/FTIR Data for DWNT with Various Surface Functionalities
(Inert Atmosphere)

Sample name	1 st Mass loss (%)	2 nd Mass loss (%)	FC _A (wt %)	FC _T (wt %)	TC _{mass} (wt %)	Effective functionalization (mmol of TDI- C_X /mg of CNT)
pDWNT	NA	NA	3.2	NA	NA	NA
pDWNT-TDI- CH_3	2.1	2.7	4.8	14.7	32.6	2.7 e-4
pDWNT-TDI- C_{12}	4.2	1.7	5.9	24.6	24.0	1.8 e-4
pDWNT-TDI- C_{18}	2.5	3.4	5.9	28.7	20.5	1.5 e-4

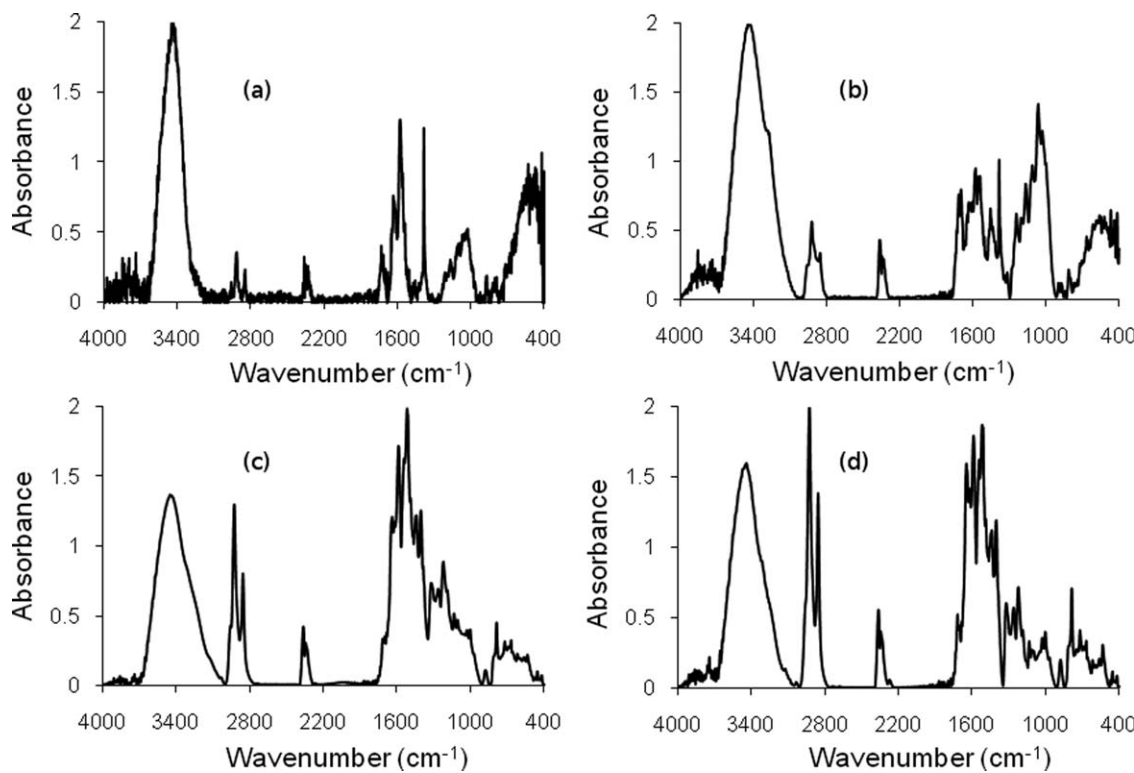


Figure 10 FTIR spectrum of DWNT. (a) DWNT-TDI-CH₃; (b) DWNT-TDI-C₁₂; and (c) DWNT-TDI-C₁₈ sample.

The peaks at 2920 cm⁻¹ and 2850 cm⁻¹ showed a slight increase in intensity (compared with the broad H₂O peak at ~ 3440 cm⁻¹) indicating more CH₂ groups were present. There was also a significant shoulder to the 2920 cm⁻¹ peak (at 2950 cm⁻¹) that implied the presence of CH₃ groups, further confirmation that the reaction proceeded as described.

Both the DWNT-TDI-C₁₂ sample [Fig. 10(c)] and DWNT-TDI-C₁₈ sample [Fig. 10(d)] exhibited peaks at 1617 cm⁻¹ and 1540 cm⁻¹, which were assigned to the Amide I and II vibrations in the amide linkage shown in Figure 1. The peak at 1635 cm⁻¹ was assigned to the vibrations of the carbonyl group in the urea linkage, whereas the peak at 1222 cm⁻¹ was assigned to C—N vibrations in the urea linkage. The presence of these two peaks in combination with an increase in intensity of the C—H peaks at 2920 cm⁻¹ and 2850 cm⁻¹ (compared with the broad H₂O peak

at 3440 cm⁻¹) confirmed the reaction schemes in Figures 1 and 2.

It was originally hypothesized that covalent attachment of TDI-based functional groups to CNT sidewalls and end caps would increase tensile properties of the TPU nanocomposite through a combination of increased polymer/CNT interfacial interaction and increased CNT dispersion. It was further hypothesized that an increase in CNT functional group length would increase the tensile properties of the TPU nanocomposites through increased dispersion of individual CNT. With the noted exception of the TPU/DWNT-TDI-C₁₂ nanocomposite, the tensile data (summarized in Table III) appeared to fit these hypotheses with tensile strength generally increasing both as a result of the addition of functional groups to the CNT surface and as the functional group alkyl chain length increased.

TABLE III
Summary of Tensile Data for TPU Nanocomposites Containing DWNT with Various Surface Functionalities

Sample	Tensile strength (MPa)	Young's modulus (MPa)	Strain at break (%)	Toughness (MPa)
Host TPU	22.3 ± 6.0	5.0 ± 0.7	913.3 ± 113.1	68 ± 19
TPU/pDWNT (1%)	24.3 ± 3.1	5.6 ± 0.3	914.1 ± 117.4	64 ± 22
TPU/pDWNT-TDI-CH ₃ (1%)	29.8 ± 4.7	5.2 ± 1.1	872.6 ± 143.6	90 ± 14
TPU/pDWNT-TDI-C ₁₂ (1%)	26.5 ± 2.6	6.4 ± 0.9	821.5 ± 51.3	81 ± 8
TPU/pDWNT-TDI-C ₁₈ (1%)	32.1 ± 4.5	3.2 ± 0.9	896.8 ± 6.5	97 ± 14

The TPU/DWNT-TDI-C-H₃ nanocomposite showed a 23% increase in tensile strength when compared with the TPU/DWNT nanocomposite and a 34% increase when compared with the host TPU. Young's modulus remained relatively constant when compared with both the host TPU and TPU/DWNT samples. These results suggest that the addition of functional groups to DWNT has increased polymer/DWNT interfacial interactions and/or increased dispersion of individual DWNT.

The best performed nanocomposite, TPU/DWNT-TDI-C₁₈, showed a 32% increase in tensile strength when compared with the unfunctionalized TPU/DWNT nanocomposite and a 44% increase in tensile strength compared with the host TPU. This was considered a significant result considering this sample contained fewer CNT than the TPU/DWNT nanocomposite. Notably, this increase in tensile strength was not accompanied by a significant increase in Young's modulus, in fact the modulus actually decreased by 36%. This data may suggest that individual DWNT-TDI-C₁₈ were selectively reinforcing the TPU hard domains. Theoretically, preferential CNT reinforcement of soft domains would act to increase bulk modulus similar to an increase in hard segment content of the host TPU. Differential scanning calorimetry data (not shown) demonstrated that the addition of CNT, whether functionalized or not, had no influence on either the hard segment crystallinity or the phase separation of the hard and soft domains. Selective CNT interaction with the hard domains, however, would have minimal impact on modulus, allowing the initial elastic deformation of the soft domains under low strain while still allowing the CNT to take a disproportionately large share of the applied load, thus increasing tensile strength at much higher strains. Hence, it was thought the increased dispersion resulting from steric hindrance of the larger functional groups increased the number of individual CNT interacting with the host polymer. The larger functional moiety also allowed some interaction with the soft domains in those regions along the nanotube length where phase boundaries were crossed.

CONCLUSIONS

Double walled carbon nanotubes were functionalized with several functional groups of varying size through

a two-stage reaction procedure. TGA coupled with FTIR analysis of both the decomposition products and the actual samples demonstrated that the functionalization procedure was successful and proceeded as expected. A preliminary investigation of the reinforcing capabilities of the functionalized CNT in a TPU-based nanocomposite demonstrated that all functionalized CNT provided superior reinforcement compared with both the host TPU and the unfunctionalized DWNT control samples. Furthermore, the octadecylamine functionality provided the greatest enhancement in tensile strength in agreement with the initial hypotheses.

References

- Lin, Y.; Taylor, S.; Li, H. P.; Fernando, K. A. S.; Qu, L. W.; Wang, W.; Gu, L. R.; Zhou, B.; Sun, Y. P. *J Mater Chem* 2004, 14, 527.
- Qiu, H. X.; Shi, Z. J.; Guan, L. H.; You, L. P.; Gao, M.; Zhang, S. L.; Qiu, J. S.; Gu, Z. N. *Carbon* 2006, 44, 516.
- Coleman, J. N.; Khan, U.; Blau, W. J.; Gun'ko, Y. K. *Carbon* 2006, 44, 1624.
- Grujicic, M.; Sun, Y. P.; Koudela, K. L. *Appl Surf Sci* 2007, 253, 3009.
- Lordi, V.; Yao, N. *J Mater Res* 2000, 15, 2770.
- Sen, R.; Zhao, B.; Perea, D.; Itkis, M. E.; Hu, H.; Love, J.; Belyarova, E.; Haddon, R. C. *Nano Lett* 2004, 4, 459.
- Sahoo, N. G.; Jung, Y. C.; Yoo, H. J.; Cho, J. W. *Macromol Chem Phys* 2006, 207, 1773.
- Kuan, H. C.; Ma, C. C. M.; Chang, W. P.; Yuen, S. M.; Wu, H. H.; Lee, T. M. *Compos Sci Technol* 2005, 65, 1703.
- Deng, J.; Zhang, X.; Wang, K.; Zou, H.; Zhang, Q.; Fu, Q. *J Membr Sci* 2007, 288, 261.
- Hilding, J.; Grulke, E. A.; Zhang, Z. G.; Lockwood, F. J. *Dispersion Sci Technol* 2003, 24, 1.
- Zhao, C. G.; Ji, L. J.; Liu, H. J.; Hu, G. J.; Zhang, S. M.; Yang, M. S.; Yang, Z. Z. *J Solid State Chem* 2004, 177, 4394.
- Liu, C.; Cong, H. T.; Li, F.; Tan, P. H.; Cheng, H. M.; Lu, K.; Zhou, B. L. *Carbon* 1999, 37, 1865.
- Li, L. X.; Li, F.; Liu, C.; Cheng, H. M. *Carbon* 2005, 43, 623.
- Niyogi, S.; Hamon, M. A.; Perea, D. E.; Kang, C. B.; Zhao, B.; Pal, S. K.; Wyant, A. E.; Itkis, M. E.; Haddon, R. C. *J Phys Chem B* 2003, 107, 8799.
- Smart, S. K.; Ren, W. C.; Cheng, H. M.; Lu, G. Q.; Martin, D. J. *Int J Nanotechnol* 2007, 4, 618.
- Szleifer, I.; Yerushalmi-Rozen, R. *Polymer* 2005, 46, 7803.
- Arepalli, S.; Nikolaev, P.; Gorelik, O.; Hadjiev, V. G.; Bradlev, H. A.; Holmes, W.; Files, B.; Yowell, L. *Carbon* 2004, 42, 1783.
- Belin, T.; Epron, R. *Mater Sci Eng B-Solid State Mater Adv Technol* 2005, 119, 105.
- Hesse, M.; Meier, H.; Zeeh, B. *Spectroscopic Methods in Organic Chemistry*. Thieme Foundations of Organic Chemistry Series; G. Thieme: New York, 1997; p 365.
- Zhang, Y. J.; Li, J.; Shen, Y. F.; Wang, M. J.; Li, J. H. *J Phys Chem B* 2004, 108, 15343.